

Particle-number conservation in static-path approximation for thermal superfluid systemsK. Kaneko^{1,*} and A. Schiller²¹*Department of Physics, Kyushu Sangyo University, Fukuoka 813-8503, Japan*²*National Superconducting Cyclotron Laboratory, Michigan State University, East Lansing, Michigan 48824, USA*

(Received 1 May 2007; published 6 December 2007)

By applying particle-number projection to the static-path approximation (SPA), the heat capacity and the breakdown of pairing correlations are investigated in the thermally excited, superfluid systems ^{172}Yb , ^{94}Mo , and ^{56}Fe . For the heavy nucleus ^{172}Yb , the heat capacities in both the SPA and the number-projected SPA (NPSPA) exhibit an \mathcal{S} shape; the difference between the SPA and NPSPA heat-capacity curves is not very large and the particle-number projection thereby enhances the \mathcal{S} shape already seen in the SPA. The temperature at which the \mathcal{S} -shape of heat capacity curve occurs parallels the temperature of the breakdown of pairing correlations as indicated by the effective pairing gap. However, for the comparatively lighter nuclei ^{94}Mo and ^{56}Fe , the SPA does not produce an \mathcal{S} -shaped heat capacity on its own; only after particle-number projection the \mathcal{S} shape appears in the heat-capacity curve. For ^{94}Mo , we compare the NPSPA result with thermal odd-even mass differences, which are regarded as a direct measure of the pairing gap.

DOI: [10.1103/PhysRevC.76.064306](https://doi.org/10.1103/PhysRevC.76.064306)

PACS number(s): 21.60.Jz, 21.10.Ma, 05.30.-d, 27.70.+q

I. INTRODUCTION

Pairing correlations are of special importance for many-fermion systems such as electrons in superconducting metals, nucleons in the nucleus, and quarks in color superconductivity. The Bardeen-Cooper-Schrieffer (BCS) theory [1] of superconductivity has successfully described the sharp superfluid-to-normal phase transition connected to the breakdown of pairing correlations for an infinite Fermi system. Such a second-order phase transition is characterized by a discontinuity of the second derivative of the partition function with respect to some order parameter, e.g., in the present case, a jump of the heat capacity at a critical temperature. For finite Fermi systems, however, recent theoretical approaches [2–5] demonstrate that thermal and quantal fluctuations are important; they wash out the discontinuity of the heat capacity which is obtained in the BCS approximation, and instead produce a continuous \mathcal{S} -shape around the critical temperature. Such an \mathcal{S} -shape has been found experimentally by the Oslo group [6,7], and interpreted as a signature of the pairing phase transition. Another fingerprint of this transition is the local decrease of thermal odd-even mass differences [8–10] extracted from the observed level densities of a triplet of isotopes with neutron number $N - 1$, N , and $N + 1$, which yields a temperature corresponding to the one obtained from the \mathcal{S} shape of the heat capacity curve.

In finite Fermi systems such as nuclei, the BCS theory alone fails to provide a good approximation of thermal properties. This comes because particle number is not a good quantum number in the BCS description of the superfluid phase. Indeed, a BCS treatment with rigorous number projection [11] such as the variation after projection (VAP) method [11,12] smooths out the sharp phase transition and hence gives a more realistic picture, while the discontinuity in the heat capacity remains in, e.g., the projection after variation (PAV)

method [11,13–15]. Exact number projection is also essential for an accurate description of odd-even effects seen in the heat-capacity curves of small superfluid systems. It is therefore desirable to investigate how the number projection affects thermal properties such as the \mathcal{S} shape in heat capacity of nuclei [12,16]. In particular, it has been recently demonstrated [16], that particle-number projection within the BCS theory by the PAV scheme can produce an \mathcal{S} -shaped heat capacity even in the absence of a pairing-phase transition, i.e., when assuming a constant pairing gap at all temperatures due to the effect of particle-number conservation on quasiparticle excitations. In general, this method produces both an \mathcal{S} -shaped heat capacity due to the effect of particle-number projection and a discontinuity in the heat capacity related to the pairing phase transition.

Inclusion of fluctuations and correlations beyond the BCS theory as induced by, e.g., exact particle number projection, can be done starting with the path-integral representation of the partition function. A direct approach to evaluate the path integral is the shell-model Monte Carlo method [3–5]. However, the computational effort is quite large, and it cannot be applied to the large shell-model spaces typical for heavy nuclei. The static-path approximation (SPA) [13,17–19] is therefore a useful treatment to evaluate approximately the partition function in finite systems with separable interactions. In recent theoretical approaches, also small-amplitude fluctuations around the static path have been taken into account. These fluctuations give corrections to the partition function similar to the standard random-phase approximation around the mean field. Thus, the static-path plus random-phase approximation (SPA+RPA) method for interactions and temperature regions applied in [2,20–22] gives excellent agreement with exact results [2]. In this paper, we will perform the exact number projected SPA (NPSPA), since the SPA results for the \mathcal{S} -shaped heat capacity qualitatively agree with the SPA+RPA ones [23]. For this, we employ thermofield dynamics (TFD) [24,25], which is a powerful tool for describing many-body systems at finite temperature.

*kaneko@ip.kyusan-u.ac.jp

II. METHOD

In this work, we consider a monopole pairing Hamiltonian

$$\hat{H} = \sum_{k,\tau} \varepsilon_{k,\tau} (\hat{c}_{k,\tau}^\dagger \hat{c}_{k,\tau} + \hat{c}_{\bar{k},\tau}^\dagger \hat{c}_{\bar{k},\tau}) - \sum_{\tau} G_{\tau} \hat{P}_{\tau}^\dagger \hat{P}_{\tau}, \quad (1)$$

with the time reversed states \bar{k} , and the pairing force strength G_{τ} , where $\tau = \pi, \nu$ stands for protons and neutrons, respectively. Here, $\varepsilon_{k,\tau}$ are the single-particle energies and \hat{P}_{τ} is the pairing operator $\hat{P}_{\tau} = \sum_k \hat{c}_{k,\tau} \hat{c}_{k,\tau}$.¹

By means of the number-projected SPA [2,13] based on the Hubbard-Stratonovich transformation [26], the canonical partition function is given by

$$\begin{aligned} Z_N &= \text{Tr}[\hat{P}_N e^{-\beta \hat{H}'}]_{\text{SPA}} \\ &= \frac{2}{GT} \int_0^\infty d\Delta \Delta e^{-\Delta^2/GT} Z_N(\Delta), \end{aligned} \quad (2)$$

with

$$Z_N(\Delta) = \text{Tr}[\hat{P}_N e^{-\beta \hat{h}(\Delta)}], \quad (3)$$

$$\hat{h}(\Delta) = \sum_k \varepsilon'_k (\hat{c}_k^\dagger \hat{c}_k + \hat{c}_{\bar{k}}^\dagger \hat{c}_{\bar{k}}) - \Delta (\hat{P}^\dagger + \hat{P}) + \frac{G\Omega}{2}, \quad (4)$$

where $\hat{H}' = \hat{H} - \mu \hat{N}$, $\hat{N} = \sum_k \hat{c}_k^\dagger \hat{c}_k$ is the particle-number operator, and μ is the chemical potential. Furthermore, \hat{P}_N is the exact number projection defined by

$$\hat{P}_N = \frac{1}{2\pi} \int_0^{2\pi} d\varphi e^{-i\varphi(\hat{N}-N)}, \quad (5)$$

and we define for later $\lambda_k = \sqrt{\varepsilon_k'^2 + \Delta^2}$ with $\varepsilon_k' = \varepsilon_k - \mu - G/2$. Then, the thermal energy can be calculated from $E = -\partial \ln Z_N / \partial \beta$. It is now convenient to introduce quasiparticles by diagonalizing the Hamiltonian of Eq. (4)

$$\begin{pmatrix} \hat{a}_k \\ \hat{a}_k^\dagger \end{pmatrix} = \mathcal{W}^\dagger \begin{pmatrix} \hat{c}_k \\ \hat{c}_k^\dagger \end{pmatrix} = \begin{pmatrix} u_k^* & v_k^* \\ v_k & u_k \end{pmatrix} \begin{pmatrix} \hat{c}_k \\ \hat{c}_k^\dagger \end{pmatrix}, \quad (6)$$

where the matrix satisfies unitarity $\mathcal{W}^\dagger \mathcal{W} = 1$. The matrices u and v in Eq. (6) diagonalize the pairing term of Eq. (4). They are diagonal and determined by solving the Hartree-Fock-Bogoliubov (HFB) equations

$$\begin{pmatrix} \varepsilon_k' & \Delta \\ \Delta & -\varepsilon_k' \end{pmatrix} \begin{pmatrix} u_k \\ v_k \end{pmatrix} = \lambda_k \begin{pmatrix} u_k \\ v_k \end{pmatrix}, \quad (7)$$

where λ_k is the quasiparticle energy.

To evaluate the partition function $Z_N(\Delta)$ in Eq. (3), we employ the treatment of number projection [14] using the TFD formalism [24,25]. The TFD is known to be a powerful tool for a perturbative treatment within thermal mean-field theory [27]. The thermal expectation value of an observable is thereby expressed in terms of a vacuum expectation value in an enlarged space. The advantage of the TFD is that the thermal average of an arbitrary operator can be easily handled in a similar manner as the expectation value in the zero-temperature formalism. In TFD, the Hilbert space spanned by the quasiparticle operators is doubled by including

a fictitious (tilde) operator $\{\hat{\tilde{a}}_k, \hat{\tilde{a}}_k^\dagger\}$. Then, the quasiparticle vacuum is doubled by the corresponding vacuum $|0\rangle$ defined as $\hat{a}_k|0\rangle = \hat{\tilde{a}}_k|0\rangle = 0$. Next, we introduce the temperature-dependent operators and vacuum by the unitary transformation

$$\hat{a}_k(\beta) = e^{-i\hat{G}} \hat{a}_k e^{i\hat{G}}, \quad (8)$$

$$\hat{\tilde{a}}_k(\beta) = e^{-i\hat{G}} \hat{\tilde{a}}_k e^{i\hat{G}}, \quad (9)$$

$$|0(\beta)\rangle = e^{-i\hat{G}} |0\rangle, \quad (10)$$

where the generator \hat{G} is given by

$$\hat{G} = i \sum_k \theta_k (\hat{a}_k^\dagger \hat{\tilde{a}}_k^\dagger - \hat{\tilde{a}}_k \hat{a}_k). \quad (11)$$

Here, θ_k is the angle of the transformation. The Fock space is spanned by the set of operators $\{\hat{a}_k^\dagger(\beta), \hat{\tilde{a}}_k^\dagger(\beta)\}$ and the vacuum $|0(\beta)\rangle$. The transformations in Eqs. (8) and (9) can also be rewritten as

$$\begin{pmatrix} \hat{a}_k \\ \hat{\tilde{a}}_k^\dagger \end{pmatrix} = \begin{pmatrix} \cosh \theta_k & \sinh \theta_k \\ \sinh \theta_k & \cosh \theta_k \end{pmatrix} \begin{pmatrix} \hat{a}_k(\beta) \\ \hat{\tilde{a}}_k^\dagger(\beta) \end{pmatrix}. \quad (12)$$

With this, the thermal average of an arbitrary operator \hat{A} is expressed as the expectation value with respect to the temperature-dependent vacuum $|0(\beta)\rangle$ by

$$\begin{aligned} \langle \hat{A} \rangle &= \text{Tr}(\hat{A} e^{-\beta \hat{H}}) / \text{Tr}(e^{-\beta \hat{H}}) \\ &= \langle 0(\beta) | \hat{A} | 0(\beta) \rangle, \end{aligned} \quad (13)$$

where \hat{H} is the full Hamiltonian of the system. To determine the angle parameter θ_k , we evaluate the thermal average of the number operator $\hat{a}_k^\dagger \hat{a}_k$ with respect to $|0(\beta)\rangle$ as

$$\langle 0(\beta) | \hat{a}_k^\dagger \hat{a}_k | 0(\beta) \rangle = \sinh^2 \theta_k. \quad (14)$$

Since the left-hand of Eq. (14) should give the Fermi distribution function, the angle is chosen as

$$f_k = \sinh^2 \theta_k = \frac{1}{e^{\beta \lambda_k} + 1}. \quad (15)$$

Using the definition of the thermal average from Eq. (13), the partition function $Z_N(\Delta)$ in Eq. (3) can be rewritten as

$$\begin{aligned} Z_N(\Delta) &= \text{Tr}[\hat{P}_N e^{-\beta \hat{h}(\Delta)}] \\ &= \text{Tr}(e^{-\beta \hat{h}(\Delta)} |0(\beta)\rangle \langle 0(\beta)| \hat{P}_N |0(\beta)\rangle), \end{aligned} \quad (16)$$

with

$$\text{Tr}(e^{-\beta \hat{h}(\Delta)}) = \frac{1}{2} \prod_k e^{-(\varepsilon_k - \mu - \lambda_k)/T} (1 + e^{-\lambda_k/T})^2. \quad (17)$$

The expectation value $\langle 0(\beta) | \hat{P}_N | 0(\beta) \rangle$ can be evaluated using the TFD technique [14] in a way similar as in the zero-temperature formalism [28]. For instance, by applying the general formalism of projection [14], we can obtain the expectation value of the operator $e^{-i\hat{S}}$ by

$$\langle 0(\beta) | e^{-i\hat{S}} | 0(\beta) \rangle = (\det U)^{\frac{1}{2}} \exp \left[-i(S^{(0)} + \frac{1}{2} \text{Tr} S^{(1)}) \right], \quad (18)$$

where \hat{S} is defined as the one-body operator $\hat{S} = \varphi \hat{N}$ in the quasiparticle representation

$$\hat{S} = S^{(0)} + \sum_{kk'} S_{kk'}^{(1)} \hat{a}_k^\dagger \hat{a}_{k'} + \frac{1}{2} \sum_{kk'} [S_{kk'}^{(2)} \hat{a}_k^\dagger \hat{a}_{k'}^\dagger + \text{h.c.}], \quad (19)$$

¹Hereafter, the index τ is dropped for convenience.

with

$$S^{(0)} = \langle 0(\beta) | \hat{S} | 0(\beta) \rangle, \quad (20)$$

$$S_{kk'}^{(1)} = \langle 0(\beta) | [\hat{a}_k, \hat{S}] \hat{a}_{k'}^\dagger | 0(\beta) \rangle, \quad (21)$$

$$S_{kk'}^{(2)} = \langle 0(\beta) | \hat{a}_k [\hat{a}_{k'}, \hat{S}] | 0(\beta) \rangle, \quad (22)$$

and where U is given by the transformation

$$\exp(-i\hat{S})\hat{a}_k \exp(i\hat{S}) = \sum_{kk'} (U_{kk'}\hat{a}_{k'} + V_{kk'}\hat{a}_{k'}^\dagger). \quad (23)$$

As mentioned above, the SPA can avoid the sharp phase transition, which appears in the simple BCS approximation. To explain this, we use the saddle-point approximation for the integral of Eq. (2), where we take into account the measure Δ when the maximum of the integrand is determined. Neglecting the number projection for the sake of simplicity, the effective BCS approximation (EBCS) [30] is obtained in this way. This leads to an effective value Δ_0 which is determined by

$$\Delta_0 = G \langle 0(\beta) | \hat{P} | 0(\beta) \rangle + \frac{1}{2}GT/\Delta_0, \quad (24)$$

together with the condition for the particle number

$$N = \sum_{k>0} [1 - (u_k^2 - v_k^2) \tanh(\beta\lambda_k/2)]. \quad (25)$$

These equations are nonlinear and have to be solved by iteration in a similar way as the usual BCS equations. The solution of the above equations is a smooth, nonvanishing function of T . The second term in Eq. (24) prevents the solution from falling into the normal phase. Now, we introduce the effective pairing gap as

$$\Delta_E(T) = G \langle 0(\beta) | \hat{P} | 0(\beta) \rangle = \Delta_0 - GT/2\Delta_0. \quad (26)$$

Here, one can see that if one neglects the second term in Eq. (24), the EBCS equation is reduced to the usual BCS equation. In this sense, the second term in Eq. (24) washes out the discontinuity of the heat capacity and avoids the vanishing pairing gap at the critical temperature in the BCS theory. Such a behavior is similar to the one seen in the BCS treatment with number projection using the VAP scheme, where the sharp phase transition at the critical temperature is smoothed out.

The expectation value $\langle 0(\beta) | P_N | 0(\beta) \rangle$ in Eq. (16) can now be evaluated using the M -point formula

$$\begin{aligned} \langle 0(\beta) | \hat{P}_N | 0(\beta) \rangle &= \frac{1}{2\pi} \int_0^{2\pi} d\varphi e^{i\varphi N} \langle 0(\beta) | e^{-i\varphi \hat{N}} | 0(\beta) \rangle \\ &\cong \frac{1}{M+1} \sum_{m=0}^M e^{i\varphi_m N} \langle 0(\beta) | e^{-i\varphi_m \hat{N}} | 0(\beta) \rangle, \end{aligned} \quad (27)$$

where $\varphi_m = 2\pi m/(M+1)$ and M is the number of single particle states [28]. In the case $M=1$, the number projection is reduced to the number-parity projection [2,16].

III. RESULTS AND DISCUSSION

In this work, we consider ^{172}Yb , ^{94}Mo , and ^{56}Fe for numerical calculations. For these calculations, we use the single-particle energies ε_k given by a deformed Woods-Saxon potential with spin-orbit interaction [31]. The Woods-Saxon

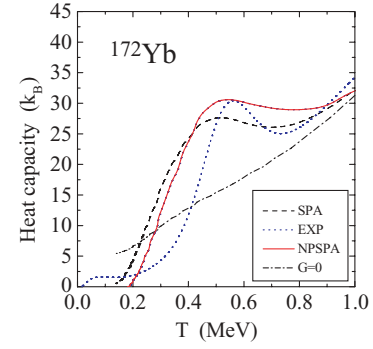


FIG. 1. (Color online) Heat capacity as a function of temperature for ^{172}Yb . The dashed and solid curves denote results from the SPA and NPSPA, respectively, the dash-dotted line gives the result for the independent-particle model, i.e., for $G=0$. Experimental data (dotted line) are taken from [6]. Good qualitative agreement between the experiment and the calculations is achieved. The temperature around the local maximum of the C_V curve coincides well between the experiment and the NPSPA.

parameters are chosen such as to approximately reproduce the experimental single-particle energies extracted from the energy levels of ^{133}Sn (^{132}Sn core plus one neutron) for ^{172}Yb , where $V_0 = 51.0$ MeV, $a = 0.67$ fm, $\kappa = 0.67$, $\lambda = 22.0$, and $r_0 = 1.27$ fm. For ^{94}Mo and ^{56}Fe , we adopt the same parameters as ones used in Ref. [10]. The doubly-degenerate single-particle levels with negative energies are taken outside of the ^{132}Sn core for ^{172}Yb , and outside of the ^{40}Ca core for ^{94}Mo and ^{56}Fe . The pairing force strengths are chosen such as to reproduce the experimental odd-even mass differences at zero temperature.

Figure 1 shows the heat capacities calculated in the SPA and number-projected SPA (NPSPA) for ^{172}Yb . This heat capacity is obtained by $\partial E/\partial T$ where E is the thermal energy given by $E = -\partial \ln Z_N/\partial\beta$. One can see that the heat capacity exhibits an S shape around $T = 0.5$ MeV [6]. The number projection decreases the SPA heat capacity for $T < 0.35$ MeV and increases it in the region of $0.35 \text{ MeV} < T < 0.7$ MeV, and hence enhances the S shape. It is important to note that an S -shaped heat capacity is already obtained within the SPA, without any number projection. To emphasize this point, we also show in Fig. 1 the heat capacity obtained from an independent-particle model without pairing, i.e., for $G=0$. As it should for a non-interacting Fermi gas, this heat capacity depends almost linearly on temperature. The difference between the heat-capacity curves of the independent-particle model and the full model treated within the SPA is large and qualitative. On the other hand, the difference between the SPA and NPSPA results is relatively smaller and quantitative in nature. When compared to experiment, the NPSPA can describe well the S -shape of the data, while the calculated C_V curve deviates from the experimental one for temperatures below 0.5 MeV. This difference may be a drawback of the SPA approximation and of the simple model used with only a monopole pairing interaction and without any other interaction. As shown in Fig. 2 for ^{94}Mo and in Fig. 3 for ^{56}Fe , however, the SPA does not produce an S -shaped heat capacity by itself in those cases; the S shape appears only in the NPSPA. A recent analysis of

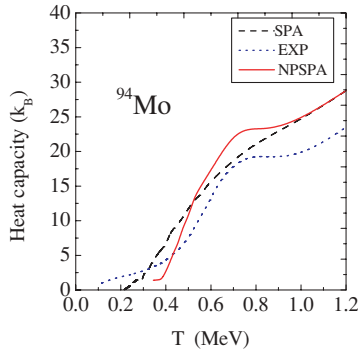


FIG. 2. (Color online) Heat capacity as a function of temperature for ^{94}Mo . Solid and dashed curves as in Fig. 1. Experimental data (dotted line) are taken from [29]. There is good qualitative agreement of the experimental data with the NPSPA. In particular, the temperatures of maximum local enhancement of the C_V curves over a Fermi gas agree well between the experiment and the NPSPA.

poles in the complex temperature plane [32] suggests that the pairing phase transition exists for mass $A > 100$ but not for $A < 100$. This interpretation seems to be consistent with the results obtained here.

The \mathcal{S} shape has also been discussed to be correlated with the breaking of nucleon Cooper pairs [4,9]. Therefore, we further investigate the neutron pairing properties in the calculations.² In Fig. 4, we show the neutron effective pairing gap Δ_E^n in the SPA and $\tilde{\Delta}_E^n = G \langle 0(\beta) | \hat{P}_N \hat{P} | 0(\beta) \rangle$ in the NPSPA, relative to their values at $T = 0$. The suppression of Δ_E^n is well correlated in temperature with the presence of the \mathcal{S} shape of the heat capacity in Fig. 1, consistent with the results of Refs. [4,9]. Thus, the \mathcal{S} shape in Figs. 1, 2, and 3 can be understood in terms of the suppression of the effective pairing gap and the effects of number projection. Previously, we have identified the inflection point of the effective pairing-gap curve as the temperature at which the pairing transition takes place [8]. As seen from the respective curves for ^{172}Yb in Fig. 4, this inflection point is close to the temperature 0.5 MeV

²The neutron pairing properties are very similar to the ones of proton pairing, therefore, proton pairing is not discussed separately in this work.

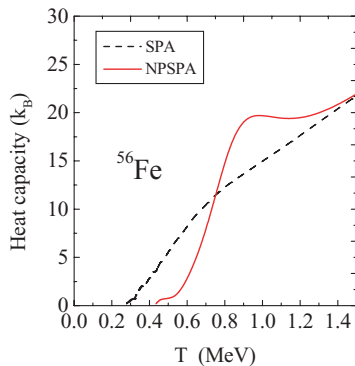


FIG. 3. (Color online) Heat capacity as a function of temperature for ^{56}Fe . Solid and dashed curves as in Fig. 1.

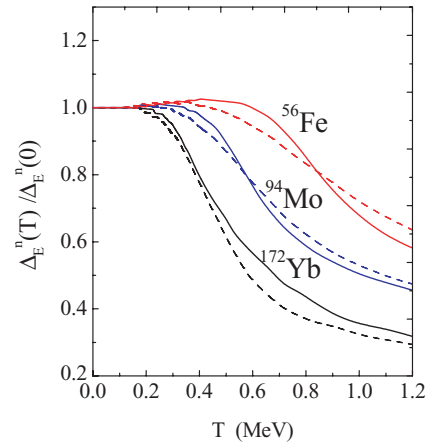


FIG. 4. (Color online) Effective pairing gap as a function of temperature for ^{172}Yb , ^{94}Mo , and ^{56}Fe . Solid and dashed curves as in Fig. 1.

at which the heat-capacity curves peak.³ For ^{94}Mo and ^{56}Fe , the respective inflection points of 0.65 MeV and 0.9 MeV are also close to the local maxima of their C_V curves.

As the experimental counterpart of the effective pairing gap, we have proposed in our previous work thermal odd-even mass differences (TOEMD) as a direct measure of the size of pairing correlations [8], and we have used them as indicators in our study of pairing phase transitions in ^{184}W [9] and $^{94-97}\text{Mo}$ [10]. We obtained in the one case a drastic in the other case a gradual decrease of the TOEMD, and we found that this signal is well correlated with the \mathcal{S} shape of the heat capacity. According to Ref. [8], the sudden decrease of the thermal odd-even mass differences is interpreted as a rapid breaking of nucleon Cooper pairs. Figure 5 shows the comparison between the effective

³To obtain a precise estimate of the inflection point, we differentiate the effective pairing-gap curves with respect to temperature.

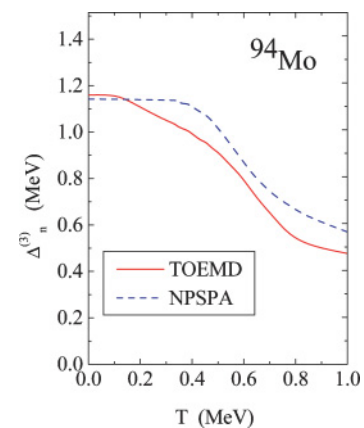


FIG. 5. (Color online) Comparison between the experimental TOEMD (solid line) extracted according to Eq. (28) and the effective neutron pairing gap (dashed line) as a function of temperature for ^{94}Mo .

pairing gap and the TOEMD defined as

$$\Delta_n^{(3)}(Z, N, T) = \frac{(-1)^N}{2} [B_t(Z, N+1, T) - 2B_t(Z, N, T) + B_t(Z, N-1, T)], \quad (28)$$

where the thermal energy B_t is defined by $B_t(Z, N, T) = E(Z, N, T) + B(Z, N)$, $B(Z, N)$ is the binding energy at zero temperature, and $E(Z, N, T)$ is evaluated from experimental level densities [9,10]. The agreement between theory and experiment is satisfying.

It is now interesting to discuss the significance of the \mathcal{S} shape of the heat capacity. For this reason, we would like to recall all the available facts. In the present work, the \mathcal{S} shape is obtained for $A > 100$ already within the SPA, while for lighter nuclei, to reproduce the \mathcal{S} shape, the NPSPA (corresponding to a VAP scheme) is needed. Interestingly, in the work of Esashika *et al.* [16], an \mathcal{S} shape could also be obtained (within a PAV scheme) when keeping the pairing gap Δ artificially constant. The latter two observations seem to indicate that the presence of the \mathcal{S} shape is not necessarily related to the pairing phase transition, and might be connected more to the particle-number projection. However, one should remember that in calculations without a distinct pairing force G , no \mathcal{S} -shaped heat capacity has been observed. Moreover, the temperature for a potential pairing phase transition derived from the \mathcal{S} -shaped heat capacity agrees very well with the temperature where pairing correlations are being suppressed (as indicated by the effective pairing gap [8]), such that a simple coincidence of the two phenomena can likely be ruled out. At present, we leave the question of the significance of the \mathcal{S} -shaped heat

capacity somewhat open, while we would like to point out that the NPSPA is certainly an important tool to investigate this problem, since it enables us to obtain an \mathcal{S} -shaped heat capacity for lighter nuclei in the first place.

IV. CONCLUSION

In conclusion, we have investigated effects of particle-number conservation in the SPA for ^{172}Yb , ^{94}Mo , and ^{56}Fe . The particle-number projection affects the \mathcal{S} shape of the heat capacity in all of these nuclei. The \mathcal{S} shape in the heat capacity of ^{172}Yb is produced by a cooperation of the quantum effects in the SPA with the effects of particle-number projection. For ^{94}Mo and ^{56}Fe , however, the \mathcal{S} shape of the heat capacity appears only in the calculation with particle-number projection, but not in the SPA alone. This observation is consistent with nuclear size effects on the existence of a pairing transition. The \mathcal{S} -shaped heat capacity from NPSPA calculations correlates well in temperature with the reduction of the effective pairing gap. The effective neutron pairing gap in ^{94}Mo is in good agreement with experimental thermal odd-even mass differences. Our treatment of the particle-number projection can be applied together with the angular-momentum projection in order to study the spin distribution of nuclear levels in such a formalism as suggested in [14]. Calculations are now in progress.

ACKNOWLEDGMENTS

Financial support from the National Science Foundation under Grant No. PHY-06-06007 is gratefully acknowledged.

-
- [1] J. Bardeen, L. N. Cooper, and J. R. Schrieffer, *Phys. Rev.* **108**, 1175 (1957).
- [2] R. Rossignoli, N. Canosa, and P. Ring, *Phys. Rev. Lett.* **80**, 1853 (1998).
- [3] S. Rombouts, K. Heyde, and N. Jachowicz, *Phys. Rev. C* **58**, 3295 (1998).
- [4] S. Liu and Y. Alhassid, *Phys. Rev. Lett.* **87**, 022501 (2001).
- [5] Y. Alhassid, G. F. Bertsch, and L. Fang, *Phys. Rev. C* **68**, 044322 (2003).
- [6] A. Schiller, A. Bjerve, M. Guttormsen, M. Hjorth-Jensen, F. Ingebreetsen, E. Melby, S. Messelt, J. Rekstad, S. Siem, and S. W. Odegard, *Phys. Rev. C* **63**, 021306(R) (2001).
- [7] E. Melby, L. Bergholt, M. Guttormsen, M. Hjorth-Jensen, F. Ingebreetsen, S. Messelt, J. Rekstad, A. Schiller, S. Siem, and S. W. Ødegård, *Phys. Rev. Lett.* **83**, 3150 (1999).
- [8] K. Kaneko and M. Hasegawa, *Nucl. Phys.* **A740**, 95 (2004).
- [9] K. Kaneko and M. Hasegawa, *Phys. Rev. C* **72**, 024307 (2005).
- [10] K. Kaneko *et al.*, *Phys. Rev. C* **74**, 024325 (2006).
- [11] C. Eseebag and J. L. Egido, *Nucl. Phys.* **A552**, 205 (1993).
- [12] H. Nakada and K. Tanabe, *Phys. Rev. C* **74**, 061301(R) (2006).
- [13] R. Rossignoli and P. Ring, *Ann. Phys. (NY)* **235**, 350 (1994).
- [14] K. Tanabe and H. Nakada, *Phys. Rev. C* **71**, 024314 (2005).
- [15] K. Tanabe, K. Sugawara-Tanabe, and H. J. Mang, *Nucl. Phys.* **A357**, 20 (1981).
- [16] K. Esashika, H. Nakada, and K. Tanabe, *Phys. Rev. C* **72**, 044303 (2005).
- [17] Y. Alhassid and J. Zingman, *Phys. Rev. C* **30**, 684 (1984); Y. Alhassid and B. W. Bush, *Nucl. Phys.* **A549**, 43 (1992).
- [18] P. Arve, G. Bertsch, B. Lauritzen, and G. Puddu, *Ann. Phys. (NY)* **183**, 309 (1988); B. Lauritzen, P. Arve, and G. F. Bertsch, *Phys. Rev. Lett.* **61**, 2835 (1988).
- [19] R. Rossignoli, A. Ansari, and P. Ring, *Phys. Rev. Lett.* **70**, 1061 (1993).
- [20] G. Puddu, P. F. Bortignon, and R. A. Broglia, *Ann. Phys. (NY)* **206**, 409 (1991); *Phys. Rev. C* **42**, R1830 (1990); G. Puddu, *ibid.* **47**, 1067 (1993).
- [21] B. Lauritzen, G. Puddu, P. F. Bortignon, and R. A. Broglia, *Phys. Lett.* **B246**, 329 (1990); B. Lauritzen, A. Anselmino, P. F. Bortignon, and R. A. Broglia, *Ann. Phys. (NY)* **223**, 216 (1993).
- [22] H. Attias and Y. Alhassid, *Nucl. Phys.* **A625**, 565 (1997).
- [23] K. Kaneko and M. Hasegawa, *Phys. Rev. C* **72**, 061306(R) (2005).
- [24] Y. Takahashi and H. Umezawa, *Collect. Phenom.* **2**, 55 (1975).
- [25] H. Umezawa, H. Matsumoto, and M. Tachiki, *Thermo Field Dynamics and Condensed States* (North-Holland, Amsterdam, 1982).
- [26] J. Hubbard, *Phys. Rev. Lett.* **3**, 77 (1959); R. L. Stratonovich, *Dokl. Akad. Nauk SSSR* **115**, 1097 (1957).

- [27] K. Tanabe and K. Sugawara-Tanabe, Phys. Lett. **B247**, 202 (1990).
- [28] K. Hara and S. Iwasaki, Nucl. Phys. **A332**, 61 (1979); **A348**, 200 (1980).
- [29] R. Chankova *et al.*, Phys. Rev. C **73**, 034311 (2006).
- [30] R. Rossignoli, Phys. Rev. C **54**, 1230 (1996).
- [31] S. Cwiok, J. Dudek, W. Nazarewicz, J. Skalski, and T. Werner, Comput. Phys. Commun. **46**, 379 (1987).
- [32] A. Schiller, M. Guttormsen, M. Hjorth-Jensen, J. Rekstad, and S. Siem, Phys. Rev. C **66**, 024322 (2002).